Published in final edited form as:
Biomaterials. 2014 November ; 35(34): 9311–9321. doi:10.1016/j.biomaterials.2014.07.057.

The promotion of functional urinary bladder regeneration using anti-inflammatory nanofibers

Matthew I. Bury[a], **Natalie J. Fuller**[a], **Jay W. Meisner**[b], **Matthias D. Hofer**[c], **Matthew J. Webber**[d,e], **Lesley W. Chow**[f], **Sheba Prasad**[a], **Hatim Thaker**[a], **Xuan Yue**[d], **Vani S. Menon**[g], **Edward C. Diaz**[a], **Samuel I. Stupp**[d,h,i,j], **Earl Y. Cheng**[a,c,d], and **Arun K. Sharma**[a,c,d,e,*]

[a]Ann & Robert H. Lurie Children's Hospital of Chicago, Division of Pediatric Urology, Chicago, IL 60614, USA

[b]Northwestern University, Evanston, IL 60208, USA

[c]Northwestern University Feinberg School of Medicine, Department of Urology, Chicago, IL 60611, USA

[d]Northwestern University, Institute for BioNanotechnology in Medicine (IBNAM), Chicago, IL 60611, USA

[e]Department of Biomedical Engineering, Evanston, IL 60208, USA

[f]Imperial College London, Royal School of Mines, Department of Materials and Institute for Biomedical Engineering, London, UK

[g]Department of Urology, Loyola University Health System, Maywood, IL 60153, USA

[h]Northwestern University, Department of Materials Science and Engineering, Evanston, IL 60208, USA

[i]Northwestern University, Department of Chemical and Biological Engineering, Evanston, IL 60208, USA

[j]Northwestern University Feinberg School of Medicine, Department of Medicine, Chicago, IL 60611, USA

Abstract

Current attempts at tissue regeneration utilizing synthetic and decellularized biologic-based materials have typically been met in part by innate immune responses in the form of a robust inflammatory reaction at the site of implantation or grafting. This can ultimately lead to tissue fibrosis with direct negative impact on tissue growth, development, and function. In order to temper the innate inflammatory response, anti-inflammatory signals were incorporated through display on self-assembling peptide nanofibers to promote tissue healing and subsequent graft

*Corresponding author. The Feinberg School of Medicine at Northwestern University, Institute for BioNanotechnology in Medicine, 303 East Superior Street, IBNAM 11-221, Chicago, IL 60611, USA. Tel.: +1 312 503 1101; fax: +1 312 503 1222. arun-sharma@northwestern.edu (A.K. Sharma)..

Appendix A. Supplementary data

Supplementary data related to this article can be found at http://dx.doi.org/10.1016/j.biomaterials.2014.07.057.

compliance throughout the regenerative process. Utilizing an established urinary bladder augmentation model, the highly pro-inflammatory biologic scaffold (decellularized small intestinal submucosa) was treated with anti-inflammatory peptide amphiphiles (AIF-PAs) or control peptide amphiphiles and used for augmentation. Significant regenerative advantages of the AIF-PAs were observed including potent angiogenic responses, limited tissue collagen accumulation, and the modulation of macrophage and neutrophil responses in regenerated bladder tissue. Upon further characterization, a reduction in the levels of M2 macrophages was observed, but not in M1 macrophages in control groups, while treatment groups exhibited decreased levels of M1 macrophages and stabilized levels of M2 macrophages. Pro-inflammatory cytokine production was decreased while anti-inflammatory cytokines were up-regulated in treatment groups. This resulted in far fewer incidences of tissue granuloma and bladder stone formation. Finally, functional urinary bladder testing revealed greater bladder compliance and similar capacities in groups treated with AIF-PAs. Data demonstrate that AIF-PAs can alleviate galvanic innate immune responses and provide a highly conducive regenerative milieu that may be applicable in a variety of clinical settings.

Keywords

Angiogenesis; Bladder tissue engineering; Inflammation; Urinary tract; Wound healing; Self-assembly

1. Introduction

The cascade of events involved in the tissue regenerative process encompasses multiple innate biological programs that aid in regeneration. These are non-exclusively comprised of a robust inflammatory reaction at the onset of tissue damage subsequently accompanied by architectural and physiological remodeling of tissue. Although the inflammatory response initially acts as a protective mechanism to aid in repair and regeneration, impediments to tissue healing including perturbations in the inflammatory response, are attributable to further tissue damage and subvert proper tissue remodeling. The expected outcome of inflammation in a normal setting is to provide a suitable environment in order to recapitulate native tissue in form and in function through a series of interdependently choreographed events encompassing several distinct phases [1].

The inflammatory response to tissue injury is in part under the control of the innate immune system. Localized tissue injury induces the onset of leukocyte invasion, edema and pain of affected tissues [2]. The tissue infiltration of leukocytes via extravasation including macrophages, granulocytes (basophils, neutrophils, mast cells, and eosinophils) has been adequately demonstrated within the field of tissue regeneration as well as cancer initiation and progression [3,4]. Neutrophils and macrophages produce pro-inflammatory cytokines and chemokines such as IL-1β, IL-6, IL-8 and TNFα. Neutrophils also possess the capacity to recruit more monocytes (and ultimately macrophages) thus continuing the cyclical process of tissue damage in a dysfunctional setting [5]. This acute inflammatory response can become chronic and eventually lead to tissue fibrosis. Abundantly fibrous tissue lacks proper physiological function as demonstrated in a number of different conditions including

the formation of adhesions following surgery, idiopathic pulmonary fibrosis, and urinary bladder tissue regeneration [3,6,7]. In order to quell the inflammatory response and promote regenerative healing, the delivery of anti-inflammatory agents may prove beneficial in this setting.

Self-assembling peptide amphiphiles (PAs) have demonstrated utility in a wide range of settings and applications [8–10]. PAs are comprised of a hydrophobic alkyl segment attached to a peptide domain that includes a β-sheet forming segment. In aqueous environments, these molecules self-assemble through hydrophobic collapse of the alkyl domain in combination with hydrogen bonding in the β-sheet domain to produce high aspect-ratio nanofibers. PAs can be synthesized to present bioactive peptide epitopes on the nanofiber surface for recognition by cell receptors or for binding to other biomolecules in order to enhance biological function in vivo [8–10]. Specific epitopes that may be of interest in the context of tissue regeneration include anti-inflammatory sequences [11]. PAs presenting anti-inflammatory epitopes at high density could potentially be utilized to modulate inflammation-based reactions in a wide array of clinical settings. Within the context of this proof-of-concept study, we have attempted to specifically ascertain whether the application of PAs expressing anti-inflammatory peptides could 1) establish a comprehensive tissue regenerative milieu and 2) modulate components of the innate inflammatory response while utilizing a highly pro-inflammatory biological scaffold known to promote tissue fibrosis in a urinary bladder augmentation model [12,13].

2. Materials and methods

2.1. Anti-inflammatory peptide amphiphile synthesis

The anti-inflammatory peptide amphiphiles (AIF-PAs) were synthesized utilizing standard fluoroen-9-ylmethoxycarbonyl (Fmoc) solid phase peptide synthesis (SPPS) procedures as previously described [8]. Briefly, the AIF-PAs were synthesized from the C-terminus to N-terminus, with Rink Amide MBHA [4-(2′,4′-Dimethoxyphenyl-Fmoc-aminmethyl)-phenoxyacetamido-methylbenzhydryl amine resin] at the C terminus as the solid state support for the addition of Fmoc-protected AA. The Fmoc group was removed by agitating the resin in a solution of 30% piperidine in dimethylformamide (DMF) (v/v) for 10 min. This step was performed twice at the beginning of each AA coupling step. This was followed by a wash with dichloromethane (DCM), two washes with DMF, and finally two final washes in DCM. A Ninhydrin test was performed to confirm the presence of an N-terminus free amine indicated by a positive color change to purple. The AA coupling cocktail consisted of a 4× molar excess of the Fmoc AA, 3.95× molar excess of O-Benzotriazole-N,N,N′,N′-tetramethyl-uronium-hexafluoro-phosphate (HBTU), and a 6× molar excess of N,N-diisopropylethylamine (DIEA) all relative to the resin. The AA, HBTU, and DIEA were dissolved in approximately 20 mL of DMF. Once the Ninhydrin test confirmed the presence of free amino termini, the AA coupling cocktail was added to the resin and agitated for a minimum of 3 h. Following agitation, the resin was washed thoroughly with DMF 3× for approximately 1 min per wash and subsequently washed with DCM twice. A final Ninhydrin test was performed to confirm the AA had been coupled successfully indicated by a no color change. The remaining AA was added as described.

Following the addition of the AA sequence, a palmitic acid (C16) tail was coupled for 2 h at 4× molar excess with 3.95× and 6× molar excess of HBTU and DIEA, respectively, dissolved in a 20:80 mixture of DCM:DMF.

To cleave the finished AIF-PA from the resin, a solution containing 95% trifluoroacetic acid (TFA), 2.5% triisopropylsilane (TIS), and 2.5% nanopure water was mixed with the resin and agitated for at least 3 h. The solution was isolated from the resin into a 500 mL round bottom flask, and the resin was washed once with DCM. The TFA was removed using a rotary evaporator (R-210; Buchi Analytical Inc.) at 50 °C. Cold diethyl ether was added to remove soluble protecting groups remaining after cleaving and precipitate the AIF-PAs. The AIF-PA diethyl ether solution was centrifuged and decanted, leaving only the AIF-PA precipitate, which was then dried under vacuum for 2 days. Following cleavage, the AIF-PAs were purified via RP-HPLC (Varian Prostar; Varian Inc.) under either acidic (C-18 Atlantis Column; Waters Corp.) or basic (C-18 Gemini Column; Phenomenx Inc.) conditions based on the net charge of the complete AIF-PA at physiological pH. Purification was monitored by UV/Vis spectroscopy at 220 nm and 325 nm. Fractions of interest were confirmed to contain the target AIF-PA via mass spectrometry (6510 Q-TOF LC/MS 1200 Series; Agilent Technologies). Following purification, the AIF-PAs were subject to rotary evaporation before being lyophilized (FreeZone Plus 6; Labconco Corp.) for 3 days. Dried samples were stored at −20 °C until needed. The AA sequences (with the bioactive epitope in bold) of the AIF-PAs utilized throughout this study were: AIF-PA1: C_{16}-VVVAAAEEE**MQMKKVLDS**; AIF-PA2: C_{16}-VVVAAAEEE**HDMNKVLDL**; AIF-PA3: C_{16}-VVVAAAEEE**KVLDPVKG**; AIF-PA4: C_{16}-VVVAAAEEE**KVLDGQDP**; AIF-PA5: C_{16}-VVVAAAEEE**DPVKG**; AIFC-PA6 (Control): C_{16}-VVVAAAEEE**KLMSQKMVD**. AIFC-PA6 expressed a scrambled AA sequence that served as a control throughout experiments. Sequences were derived from studies of the uteroglobin protein [11,14]. All chemicals were purchased from Sigma–Aldrich Corporation.

2.2. Scanning electron microscopy of SIS scaffolds

Scanning electron microscopy (SEM) was performed using a Hitachi S4800-II scanning electron microscope (Hitachi Inc.) with a 5 kV accelerating voltage. To prepare samples for imaging, a sample of SIS coated with an AIF-PA was prepared by identical methods as were used for in vivo studies. An AIF-PA solution, induced to form a gel using a $CaCl_2$ solution, was coated onto one side of the surface of an SIS scaffold. The sample was fixed in 2% glutaraldehyde and 3% sucrose in phosphate buffered saline (PBS) for 30 min at 4 °C followed by sequential dehydration in an ascending series of ethanol. The scaffold was then dried at the critical point and coated with 8 nm OsO_4 prior to imaging. Images were collected of both the SIS surface alone and a representative sample of SIS with AIF-PA on the surface.

2.3. Rat bladder augmentation model

Athymic female rats (weighing ~200 g and 8–10 weeks old; National Cancer Institute Animal Production Program) underwent bladder augmentation as previously described [15]. Athymic rats were chosen for this study to solely examine the innate immune response to inflammation without influence of the adaptive immune response. In order to induce

anesthesia, animals were given intraperitoneal injections of 60 mg/kg ketamine and 5 mg/kg xylazine. A second injection consisting of Buprenex (1 mg/kg) was administered subcutaneously to alleviate any pain/discomfort during and following surgical procedures. An approximate 1.5 cm midline vertical skin incision was created to expose the abdominal fascia and muscles. This was immediately followed by the separation of the wall leading to the identification of the bladder. An approximate 70% supratrigonal cystectomy was performed from anterior to posterior creating a clamshell. Immediately prior to bladder augmentation procedures, samples of the pro-inflammatory biological scaffold, small intestinal submucosa [SIS (0.5 × 0.5 cm); Cook Biotech.) [12,13,16] were thoroughly dip-coated separately in one of the previously described AIF-PAs following gelation procedures. The sections of SIS were dip-coated for approximately 20 s and allowed to adhere to the SIS for an additional 30 s. Dip-coating procedures were performed at room temperature in air. The cystectomized bladder defect was then augmented with: 1) SIS (non-AIF-PA coated SIS; n = 8 animals over both time-points); 2) AIF-PA1 coated SIS (denoted as SIS/AIF-PA1; n = 11 animals over both time-points); 3) AIF-PA2 coated SIS (denoted as SIS/AIF-PA2; n = 8 animals over both time-points); 4) AIF-PA3 coated SIS (denoted as SIS/AIF-PA3; n = 3); 5) AIF-PA4 coated SIS (denoted as SIS/AIF-PA4; n = 3 animals); 6) AIF-PA5 coated SIS (denoted as SIS/AIF-PA5; n = 3 animals); and 7) AIFC-PA6 coated SIS (denoted as SIS/AIFC-PA6; n = 9 animals over both time-points). AIF-PA3, AIF-PA4, and AIF-PA5 were not utilized for 5 week in vivo studies due to their lack of overall robustness with regard to various measurements taken at the 10 day time-point. The bladder was finally covered with omentum after being closed in a watertight manner utilizing 7-0 polyglactin suture. The abdominal wall was then closed in a single layer with 5-0 ethibond running suture and the skin re-approximated with 9 mm autoclips. Each group was sacrificed at 10 day and 5 week time-points. All pre- and post-animal procedures were performed in accordance with guidelines set forth and approved by the Ann & Robert H. Lurie Children's Hospital Institutional Animal Care and Use Committee (IACUC).

2.4. Histological staining and quantification of augmented SIS/tissue samples

Explanted bladder specimens encompassing the entire thickness of the bladder were isolated immediately following euthanasia and processed as previously described [15]. Briefly, specimens were fixed in a 10% buffered formalin phosphate (Fisher Scientific, Inc.) solution followed by a series of graded ethanol exchanges then embedded in paraffin (Fisher Scientific). Embedded tissues were sectioned onto glass slides at a thickness of 10 μm using a RM2125 RT Microtome (Leica) onto glass slides and subjected to staining with Masson's Trichrome (Sigma–Aldrich Corp.) reagent. The paraffin was removed from tissue containing slides using a hot plate at 62 °C for 6 min and was followed by treatment with xylenes, graded ethanol washes and DI water. Slides were placed in Bouin's solution (Sigma–Aldrich Corp.) for approximately 15 min then rinsed under running tap water. The samples were then stained 5 min with Hematoxylin and rinsed with running water and subsequently stained with Scarlet-Acid Fuchsin (Sigma–Aldrich Corp.). Slides were rinsed again with DI water and placed into a mixture of PTA/PMA, followed by Aniline Blue solution and a 1% acetic acid wash. Finally, slides were placed in 95–100% ethanol and rinsed in xylene. Following air drying, a coverslip was placed over the specimen sample and secured with Permaslip (Alban Scientific Inc).

2.5. Bladder tissue collagen quantification

Bladder tissue specimens were evaluated for collagen content by an established protocol [13,15,17]. Collagen from Trichrome stained samples was quantified digitally utilizing a Nikon Eclipse 50i Microscope (Nikon Inc.,) and Spot Advanced Imaging Software (Diagnostic Instruments). Sample images (1600 pixels × 1200 pixels, bit depth 24) were opened with Adobe Photoshop CS3 (Adobe Systems Inc.). The contrast of red pixels from blue pixels was enhanced by a two-fold elevation of magenta levels followed by a two-fold depression of cyan levels in the red and magenta spectra. This contrast was further improved by a two-fold elevation of cyan levels followed by a two-fold depression of magenta levels in the cyan and blue spectra. The selection color range tool with a fuzziness level of 115% was then used to digitally select the red or blue pixels of the entire image. Selected pixels were subsequently quantified using the image histogram tool and a muscle to collagen ratio was calculated from these values. In cases where urothelial cells, red blood cells, debris, and the SIS scaffold were present, images were edited to remove these structures to preserve a more accurate extrapolation of the collagen content from the red:blue. Areas of regenerated tissue were subjected to an average of ten, random microscopic fields to determine collagen levels at 10 day and 5 week time-points. Data was based upon ten images per animal for each group at 10 day and 5 week time-points.

2.6. Blood vessel quantification in areas of bladder tissue regeneration

Trichrome sample images were opened with Adobe Photoshop CS3 and were initially characterized utilizing a Nikon Eclipse 50i Microscope in addition to Spot Advanced Imaging Software as previously described. Vessel numbers were quantified utilizing the pen tool based upon $n = 10$ images per graft in regenerated areas. Individual vessels were selected manually and subsequently quantified using the image histogram tool to acquire pixel density for each vessel. Data is represented as mean number of vessels/mm^2 (means ± SE).

2.7. Characterization of immunofluorescence stained augmented tissues

Tissue sections comprised of SIS alone, SIS/AIF-PA1, SIS/AIF-PA2, and SIS/AIF-PA6 augmentations were subjected to immunofluorescence staining by initially undergoing antigen retrieval which consisted of 15 min of boiling in citrate buffer (0.01 M citrate solution, pH 6.0 with 0.05% Tween-20) followed by cooling at room temperature for approximately 20 min. The antibody staining process consisted of a blocking step for 15 min in bovine serum albumin (BSA, 5 mg/ml) followed by a 40 min incubation at room temperature with the primary antibody. After washing with DPBS, slides were incubated for 30 min with a secondary antibody and eventually rinsed with DPBS and air dried. Slides were mounted with Vectashield (Vector Laboratories). Primary antibodies utilized in this study were directed against epitopes for the inflammatory markers CD68 (macrophage) [18,19] MPO (neutrophil) [20] or the inflammation-related proteins IL1b, TNFα, IL-10, IL-13, CD206 (M2 macrophage) [21–25] and CD86 (M1 macrophage) [26]. Antibodies directed against the ECM in regenerating bladder tissue (including COL4A3 and fibronectin) were also utilized. Alexa Red 555 or FITC conjugated secondary antibodies (Molecular Probes) were utilized for visualization following established protocols [15].

Primary antibodies were utilized at dilutions ranging from 1:50 to 1:400, while secondary antibodies were utilized at a 1:400 dilution. All samples were additionally stained with 4′,6-diamidino-2-phenylindole (DAPI; Sigma–Aldrich Corp.) to identify cells by nuclei visualization. All primary antibodies were purchased from Abcam or Santa Cruz Biotechnology.

Immunofluorescence quantification of stained tissue sections (including granuloma characterization) was carried out utilizing a Nikon Eclipse 50i microscope and Spot Advanced Imaging software. Ten images per animal were taken within the regenerating area of the bladder for any of the aforementioned inflammatory markers. The number of percent positive inflammatory cells was determined by manually counting marked/colored cells using ImageJ (National Institutes of Health) software. The cell counter plugin function was used to mark any cells expressing a given marker. The total number of cells were determined by opening DAPI alone images with ImageJ, and converting images into 8-bit grayscale. The threshold of the imaged was then adjusted to highlight all $DAPI^+$ cells to be counted and the watershed setting was selected to separate any stacked/merged cells. Once desired cells were highlighted and separated, total cell counts were determined using the analyze particle tool, with size adjusted to 180 pixels-infinity and circularity set to 0.0–1.0.

2.8. Urodynamic testing and bladder capacity measurements of augmented bladders

The bladders of anesthetized athymic rats were exposed through the abdomen as previously described. A 20 gauge cannula (Becton Dickinson and Co.) was delicately placed into the bladder through the dome in order to obtain intravesical measurements. The cannula was connected to the Pump 11 Elite Syringe Pump (Harvard Apparatus) and to a physiological pressure transducer (SP844, MEMSCAP). The pressure transducer was connected to a bridge amplifier (Model FE221; AD Instruments). Continuous reading of the transvesical pressure was measured and plotted using LabChart 7.3 software (AD Instruments). The fill rate for each study ranged from 150 to 200uL per minute. Bladder capacity was measured by a modified version as previously described [13]. Briefly, sterile DPBS was injected into the bladder using a 27 gauge needle in 50 μl increments until fluid leakage was observed from the urethra of the animal. The total volume injected was then noted. This procedure was repeated at least three times per animal. Urine was evacuated from the bladder prior to the start of any bladder capacity measurements utilizing a sterile 27 gauge needle. Urodynamic and bladder capacity measurements were performed immediately prior to augmentation procedures and immediately prior to euthanization. Intravesical urodynamic measurements could not be performed during the time course of this study due to the highly invasive nature of the testing procedure. UDS tracings represent a minimum of three animals pre- and post-augmentation per group.

2.9. Statistical analysis

Differences between control and treatment groups were determined using ANOVA with the Tukey–Kramer method for multiple comparisons (SAS 9.4). $P < 0.05$ was considered statistically significant.

3. Results

3.1. Quantitative morphometric and histological evaluation of SIS/AIF-PA augmented tissue

The chemical structures of the AIF-PAs are provided (Fig. S1A–F). A representative scanning electron micrograph of an AIF-PA-coated small intestinal submucosa (SIS) scaffold reveals the high density of epitope-expressing nanofibers that stud the surface of the SIS scaffold (Fig. S1G). AIF-PAs 3-5 were only used for 10 day time-point studies.

Masson's Trichrome (10 days and 5 weeks) staining of augmented bladder tissue specimens demonstrated varying levels of collagen accumulation in "control samples" (SIS alone and SIS/AIFC-PA6), respectively at 10 days post-augmentation. SIS augmented samples consistently demonstrated large and dense areas of collagen (blue (in web version) in color, depicted by black arrows; Fig. 1A; column I, row 1) accrued in a disorganized manner throughout the grafts mostly devoid of cells (red (in web version) stain). Analogous results were also demonstrated with SIS/AIFC-PA6 (Fig. 1A; column I, row 2). In contrast, SIS/AIF-PA1 and SIS/AIF-PA2 ("treatment samples") exhibited lesser degrees of collagen and tissue was interspersed with encroaching cells from the native bladder (Fig. 1A; column I, rows 3 and 4). Other extra-cellular matrix tissue deposition was also examined (Fig. S2). H&E staining revealed high levels of infiltrating inflammatory cells in areas of regeneration in control samples Fig. 1A; column II, rows 1 and 2; boxed areas). SIS samples further demonstrated the formation of granulation tissue throughout the graft as demonstrated by the dense brown (in web version) staining seen in Fig. 1A (column II, row 1). Granulation tissue was evident in all samples but to a far lesser degree in treatment grafts at both time-points in both quantity and size (Fig. S3 and Table S1). The trend of collagen accumulation continued at the 5 week time-point as levels of collagen remained higher in control samples (Fig. 1A; column III, rows 1 and 2) and decreased with the treatment samples (Fig. 1A; column III, rows 3 and 4). Normal bladder architecture was also predominant in treatment grafts. Inflammatory cell populations were still present in control samples and were in limited number with treatment samples (Fig. 1A; column IV, rows 1–4). Kidney morphology appeared normal at the gross and microscopic levels (Fig. S4). Quantitative morphometric analyses of collagen and blood vessel formation revealed a disparity between control and treatment groups.

The control groups exhibited mean levels of collagen approaching 70% (10D: SIS 73.9 ± 0.2%, SIS/AIFC-PA6 71.5 ± 1.4%; 5W: SIS 69.8 ± 3.0%, SIS/AIFC-PA6 68.8 ± 2.7%) while samples in the treatment groups demonstrated mean levels of <60% (10D: SIS/AIF-PA1 59.1 ± 1.1%, SIS/AIF-PA2 58.6 ± 0.4%; 5W: SIS/AIF-PA1 55.0 ± 1.2%, SIS/AIF-PA2 58.0 ± 0.6%) (Fig. 1B) At 5 weeks, none of the groups showed a significant increase or decrease from 10 day values. At 10 days post-augmentation, regenerated tissue in treatment group grafts was significantly more vascularized than in control group grafts (vessels/mm^2, 10D: SIS 38.5 ± 3.8, SIS/AIFC-PA6 37.0 ± 2.3 vs. SIS/AIF-PA171.0 ± 1.5, SIS/AIF-PA2 71.5 ± 6.7) (Fig. 1C). All groups demonstrated an increase in vessel number over time; mean levels for control groups at 5 weeks stayed below the mean levels for treatment groups at 10 days (vessels/mm^2, 5W: SIS 60.2 ± 8.5, SIS/AIFC-PA6 53.3 ± 4.4 vs. SIS/AIF-PA1 90.7 ±

4.5, SIS/AIF-PA2 96.7 ± 4.4) (Fig. 1C). Grafted samples SIS/AIF-PA3, SIS/AIF-PA4, and SIS/AIF-PA5 demonstrated differing degrees of collagen accumulation (Fig. S5A, Table S2) and blood vessel formation (Fig. S5A, Table S2) at 10 days post-augmentation. Bladder peripheral nerve regeneration was not apparent at either time-point under any treatment condition as determined by immunofluorescence staining. This may have been due to insufficient experimental duration.

3.2. Evaluation of inflammatory cell infiltrate of grafted bladder tissue

Innate immune-derived cells are typically the first to arrive upon areas of tissue insult [27]. The presence of macrophages and neutrophils was evaluated in both control and treatment grafts. $CD68^+$ macrophages were highly abundant in control samples 10 days post-augmentation as evidenced by their intense staining (green (in web version), Fig. 2A; column I; rows 1 and 2). This staining encompassed the entirety of the graft especially along the sutured bladder perimeter at the juncture of the SIS and the native bladder tissue. This was accompanied by a localized influx of numerous MPO^+ (myeloperoxidase) neutrophils (red (in web version), Fig. 2A; column II; rows 1 and 2) to a lesser degree than macrophages, again spanning the entirety of the graft. In contrast, treatment groups qualitatively demonstrated markedly reduced levels of both cell types (Fig. 2A; columns I and II; rows 3 and 4). Although the macrophage level decreased from the 10 day to 5 week time-point, there were still significant levels of $CD68^+$ macrophages present throughout the graft in control samples (Fig. 2A; column III; rows 1 and 2) and this was decreased in treatment groups (Fig. 2A; column III; rows 3 and 4). This trend of inflammatory cell reduction was also seen with levels of MPO^+ neutrophils but was still greatest in both control graft samples (Fig. 2A; column IV; rows 1–4).

Quantitative characterization of macrophage and inflammatory markers in control and treatment samples was additionally evaluated. At 10 days post-augmentation, >60% of cells in regenerated tissue from control groups were $CD68^+$. Separately, >20% of cells stained positive for MPO and significantly lower mean positive percentages were detected in tissue from treatment groups (CD68: SIS/AIF-PA1 33.4 ± 2.0%, SIS/AIF-PA2 23.1 ± 3.3%; MPO: SIS/AIF-PA1 6.9 ± 0.7%, SIS/AIF-PA2 9.0 ± 0.5%) (Fig. 2B). By 5 weeks, mean positive percentages for CD68 and MPO in control group tissue were reduced (CD68: SIS 46.0 ± 3.9%, SIS/AIFC-PA6 42.0 ± 2.6%; MPO: SIS 17.6 ± 1.0%, SIS/AIFC-PA6 17.6 ± 1.8%), but remained higher than levels in treatment group tissue (CD68: SIS/AIF-PA1 17.6 ± 1.8%, SIS/AIF-PA2 16.5 ± 1.6%; MPO: SIS/AIF-PA1 5.2 ± 0.7%, SIS/AIF-PA2 7.2 ± 1.1%)(Fig. 2B). SIS/AIF-PA3, SIS/AIF-PA4, and SIS/AIF-PA5 grafted samples demonstrated differing degrees of inflammatory cellular infiltrate at the 10 day time-point only (Fig. S6, Table S3; 5 week time-point was not performed).

3.3. Macrophage subtype distribution in regenerating bladder tissue

Macrophage populations, including the M1 and M2 phenotypic subtypes, have the capacity to either promote or deter proper tissue regeneration [28]. Fig. 3A (columns I and II, rows 1 and 3) demonstrates dense immunofluorescence staining with CD86 (a M1 macrophage marker [26]; red) in both control groups at 10 days and 5 weeks post-augmentation, respectively, in regenerating bladder tissue. This observation is quite contrary to the

treatment groups where there is a paucity of $CD86^+$ macrophages (columns III and IV, rows 1 and 3) specifically at the 5 week time-points. Further immunofluorescence staining with CD206 [a M2 macrophage marker [16]; green (in web version)] indicates the decreased presence of $CD206^+$ macrophages at the 10 day time-point (columns I–IV; row 2) in all groups.

Assessment of shifts in $M1^+M2^-$ (termed "M1") and $M1^-M2^+$ (termed "M2") macrophage subsets from 10 days to 5 weeks demonstrated a substantial reduction in the number of M2, but not M1, cells in both control groups [**M2**: (10D) SIS 942.3 ± 49.1, SIS/AIFC-PA6 842.5 ± 18.9 vs. (5W) SIS 486.9 ± 61.2, SIS/AIFC-PA6 539.3 ± 46.7. **M1**: (10D) SIS 1354.1 ± 125.4, SIS/AIFC-PA6 986.9 ± 18.1 vs. (5W) SIS 1087.1 ± 113.7, SIS/AIFC-PA6 957.7 ± 106.2; cells/mm^2] (Fig. 3B). Continued elevation of M1 cell numbers was not evident in treatment groups. Mean levels of both M1 and M2 subpopulations were significantly lower than control group levels [(5W), **M1**: SIS/AIF-PA1 343.4 ± 45.4, SIS/AIF-PA2 389.4 ± 62.6. **M2**: SIS/AIF-PA1 301.7 ± 23.0, SIS/AIF-PA2 224.7 ± 39.0; cells/mm^2) (Fig. 3C). Specifically, M1 levels dropped considerably in the SIS/AIF-PA1 group from 10 days to 5 weeks while M2 levels were lower at 10 days and further decreased by 5 weeks. Comparatively low numbers of M1 and M2 cells were detected in the SIS/AIF-PA2 group at 10 days and remained low at 5 weeks.

3.4. Expression of inflammation-modulating cytokines in regenerated bladder tissue

Pro- and anti-inflammatory cytokines possess the ability to greatly influence tissue remodeling with both positive and negative outcomes [28,29]. The expression of pro-inflammatory cytokines IL-1β (red; in web version) and TNFα (red; in web version) was most abundant in control groups (Fig. 4A columns I and II; rows 1 and 2) and encompassed the entirety of the graft at the 10 day time-point. In complete contrast, treatment groups exhibited dramatically lesser levels of the aforementioned cytokines at the same time-point (Fig. 4A columns I and II; rows 3 and 4). The anti-inflammatory cytokines IL-10 (green; in web version) and IL-13 (green; in web version) appeared along an expression spectrum amongst groups. Augmented control groups expressed a paucity of these cytokines while treatment groups tended to have a greater localized expression in regenerating bladder tissue (Fig. 4A columns III and IV; rows 3 and 4) 10 days post-augmentation.

Regenerated tissue was also examined for the percentage of cells staining positive for the aforementioned cytokines. Distinct, antithetical cytokine profiles were apparent for control and treatment groups (Fig. 4B). At 10 days post-augmentation, control group graft tissue (SIS and SIS/AIFC-PA6, respectively) showed high levels of pro-inflammatory cytokines IL-1β and TNFα, with low levels of anti-inflammatory cytokines IL-10 and IL-13 (IL-1β: 56.7 ± 5.0%, 63.3 ± 2.4%; TNFα: 63.1 ± 2.6%, 65.1 ± 5.1%; IL-10: 22.0 ± 2.6%, 27.8 ± 3.0%; IL-13: 24.8 ± 2.5%, 28.6 ± 3.0%). In contrast, treatment group graft tissue (SIS/AIF-PA1 and SIS/AIF-PA2, respectively) showed decreased levels of IL-1β and TNFα, with elevated IL-10 and IL-13 expression (IL-1β: 28.2 ± 2.4%, 21.2 ± 2.4%; TNFα: 32.8 ± 2.5%, 26.3 ± 2.5%; IL-10: 52.0 ± 3.1%, 56.2 ± 3.4%; IL-13: 48.2 ± 2.8%, 41.2 ± 2.2%) (Fig. 4B). A decrease in cytokine expression by 5 weeks was noted but the overall cytokine profiles remained the same in that higher IL-1β and TNFα for control groups, and higher IL-10 and

IL-13 for treatment groups was observed (Fig. S7, Table S4). Cytokine expression levels of SIS/AIF-PAs 3-5 augmented tissues were not determined at 10 day or 5 week time-points.

3.5. Physiological bladder testing

Bladders underwent urodynamic testing (UDS) pre- and post-augmentation. Bladders were gradually filled with sterile saline until a bladder contraction occurred. Bladder pressures rose during the filling until bladder contractions occurred at intravesical pressures of 30–40 cm H_2O (Fig. 5, panels A, C, E, and G). This was similar for the SIS group, SIS/AIF-PA1, SIS/AIF-PA2, and SIS/AIFC-PA6 groups. Bladder augmentation with SIS alone led to no change in voiding pressures and decreased bladder compliance (decreased filling time until voiding occurred, panel B). This was similar for SIS/AIFC-PA6 in which the voiding pressures were unchanged or even slightly elevated (panel D). In contrast, augmentation with SIS/AIF-PA1 led to a decrease in intravesical pressures during voiding to approximately 25 cm H_2O (35 cm H_2O before augmentation) combined with higher bladder compliance as the prolonged filling duration shows (panel F). In animals augmented with SIS/AIF-PA2, the slope of pressure increase was also decreased indicating an improved compliance and we observed a decrease in bladder pressure during voiding as well (approximately 35 cm H_2O compared to 45 cm H_2O before augmentation). In contrast to the above, augmentation with SIS alone and augmentation with SIS/AIF-PA2 was not associated with an increase in bladder compliance or a decreased maximum pressure. Percent bladder capacity recovery was also measured (Table S5).

4. Discussion

Dysregulation of the inflammatory response due to disease, repeated tissue insult, or the use of inflammation-provoking foreign materials for tissue engineering purposes, can lead to excess extracellular matrix tissue deposition [30,31]. As this acute inflammatory response can initiate fibrogenesis, the tempering of this response during initial phases of tissue remodeling would be ideal [32]. The application of synthetic PAs expressing potent anti-inflammatory epitopes was able to modulate multiple aspects of tissue regeneration. Within the framework of this study, AIF-PA1 and AIF-PA2 were able to positively alter the regenerative landscape compared to the control AIFC-PA6 or the untreated, highly pro-inflammatory SIS biological scaffold [12,13]. Specifically, collagen distribution in regenerating tissue was significantly reduced while there was a striking increase in tissue blood vessel regeneration that consisted of functional, patent blood vessels (Fig. S8). Normal tri-layer bladder architecture was also observed in treatment groups as control groups demonstrated disorganized tissue organization even at 5 weeks post-surgery (Fig. 1A, column III). This was coupled with a striking reduction in the levels of inflammatory cells found in the grafted areas typically seen at the onset of an innate immune response to injury. Physiological bladder function was superior in AIF-PA1 animals compared to controls. This proof-of-concept study demonstrates the feasibility of utilizing anti-inflammatory agents in a highly invasively surgical setting in the presence of a foreign body which allows for functional tissue regeneration. Lastly, the examination of other inflammatory elements that comprise the innate, complement, and adaptive immune systems

must be thoroughly examined in order to gain a better understanding of the cellular and molecular events that govern the aforementioned anti-inflammatory processes.

Acute inflammation due to repetitive insult or inflammatory dysregulation is the precursor to chronic inflammatory events with the resulting byproduct ending in permanent scarring or fibrosis [33]. This process is in part caused by the accumulation of extracellular matrix products in and around regenerating tissue creating an inhospitable growth environment. In typical bladder augmentation models that utilize biologic or synthetic scaffolding material as a three-dimensional architectural foundation, the accumulation of excess collagen is a major obstacle that is typically encountered. It has been demonstrated that unseeded scaffolds contain approximately 78% collagen at 5 weeks post-augmentation with no resolution of these events as the collagen level increased to approximately 86% at the 10 week time-point of this study in a small animal model [17]. In a similar bladder augmentation setting, non-physiological collagen levels were also observed in a non-human primate model of bladder regeneration leading to tissue fibrosis [13]. The typical ratio of muscle to collagen in the bladder is approximately 1:1 across a variety of species [15,34,35]. Drastic deviation from this ratio leads to bladder dysfunction.

Secondary examples of fibrosis include the implantation of artificial organs and medical devices [36]. Soft tissue metal implants, including titanium based structures, posses a proclivity to commence inflammatory reactions resulting in tissue fibrosis [37]. Although mechanisms of inflammation are being fully delineated, it is believed that the innate immune response, particularly the M1 macrophage component, is responsible for eventual fibrosis. Therefore, it may be surmised that coating implantable devices with the AIF-PAs we describe may be beneficial in certain clinical applications by lessening localized macrophage accumulation and subsequently fibrosis. Our data further indicate that the treatment group AIF-PAs had a profound effect on the granuloma formation (a precursor to fibrosis). The frequency and size of granulomas was markedly disparate between groups (Fig. S3, Table. S1). There were approximately 10.5 granulomas observed in bladder tissue of control samples as opposed to approximately 4 in treatment groups. The numbers of granulomas subsided over time but there were still significant levels found at the 5 week time-point in the control groups. Granuloma levels found in treatment groups were drastically reduced although tissue necrosis and the core of granulomas were not observed in any setting. The lack of necrotic tissue may be an effect of the time-point in which the experiment was terminated. This data is quite compelling due to the diminutive size of the rodent bladder and its relationship to the granuloma size and frequency within the bladder.

Modulation of cytokine expression in an inflammatory environment is pivotal to proper wound healing and functional tissue regeneration. Exacerbation of tissue injury is typically due to the abundance of pro-inflammatory cytokines in regenerating tissue. IL-1β and TNFα secreted by M1 macrophages are key perpetrators and initiators of fibrogenesis [38,39]. The blockage of TNFα expression to prevent tissue damage and resulting fibrosis has been the focus of multiple clinical studies [40,41]. Bongartz et al. describe the systemic delivery of chimeric monoclonal antibodies against TNFα for patients with rheumatoid arthritis which was accompanied by serious side effects. In a similar fashion, IL-1β has also been the target of antibody therapy [42]. However, the systemic delivery of the aforementioned agents has

caused serious side effects including the increased risk malignant transformation [40]. We demonstrate the statistically significant reduction in expression of IL-1β and TNFα in treatment groups when compared to controls accompanied by the increase in the levels of the anti-inflammatory cytokines IL-10 and IL-13 (Fig. 4B). The approximate halving of IL-1β and TNFα levels at 10 days is quite cogent. We believe the dramatic decrease in pro-inflammatory cytokine expression was the result of two key features of this system. The first being the localized delivery of the AIF-PAs as the SIS was thoroughly coated immediately prior to surgery. But perhaps more importantly, were the high density of peptide epitopes expressed on the AIF-PAs (Fig. S1G). A previous study has determined that epitope expression on the nanofiber surface of PAs can be as high as 1×10^{14} epitopes/cm^2 [10]. This allows for concentrated delivery of the AIF-PAs in a given tissue area that could outperform any type of liquid or most other solid state delivery vehicles. Lengthier time-points within this system need to be examined to study the full range of effects of these AIF-PAs.

The ability to recreate physiologically relevant organ function following substantial insult is the major goal of regenerative medicine based strategies. UDS testing provided physiological bladder data in the form of bladder pressures and voiding patterns of regenerating bladder tissue. Proximate measurements including bladder capacity determinations pre- and post-surgery help contribute to the understanding of the intricate relationship between architectural bladder tissue regeneration and physiological function. In typical pathologic bladders, high intravesical pressures due to uninhibited contractions or high voiding pressures are associated with kidney damage due to reverse transduction of the pressure [43]. SIS/AIF-PA1 and SIS/AIF-PA2 demonstrated a decreased slope of the filling curve indicating an increase in compliance of the bladder as filling volume changes which led to a slower rise in intravesical pressures. A decrease of intravesical pressures was also observed during voiding thus fulfilling the demands of a successful augmentation. In contrast, augmentation with SIS alone and SIS/AIFC-PA6 failed to decrease intravesical pressures. We speculate that coating SIS with AIF-PA1 or AIF-PA2 is associated with an improved incorporation of the SIS into the bladder environment that promotes timely development of newly formed native tissue along the SIS. Lastly, the AIF-PAs were also able to limit bladder stone formation possibly through modulation of inflammatory cytokine expression (Fig. S9, Table S5) [44]. Physiological testing data indicate that AIF-PA coated SIS can successfully be employed for bladder augmentations leading to an improved pressure profile during filling and voiding.

Constituents of the inflammatory response to tissue injury involve both innate (including the complement system) and adaptive arms of the immune system that can either contribute to the resolution of volatile or dysfunctional tissue inflammatory responses or exacerbate the process leading to the formation of scar tissue [45,46]. The latter process is seen in a number of organ systems including those urological in nature and those relevant to cardiac repair post-myocardial infarction [47,48]. In this specific setting, regulatory T-lymphocytes have been demonstrated to attenuate the inflammatory response following a major myocardial infarct in order to prevent unfavorable tissue remodeling events through pro-inflammatory cytokine inhibition of cardiomyocytes [49]. There is considerable functional overlap with regard to the role of T-lymphocytes in the inflammatory response [50–53]. However, in

order to solely study the early innate immune response with regard to inflammation, we specifically chose the T-lymphocyte deficient animal model in order to gain better insight into the precise role this arm of the immune system may play without interference of the T-lymphocyte response. This may become especially relevant in clinical conditions in which T-lymphocyte function is aberrant/non-functional, thus negatively affecting wound healing and resulting in heavy reliance upon the innate immune response.

5. Conclusion

We have demonstrated that the application of AIF-PAs in a bladder regenerative setting possess the ability to assuage the innate immune response and promotes anatomically correct and physiologically functional bladder tissue. The supplementation of SIS biological scaffolds with AIF-PA1 and AIF-PA2 greatly reduced collagen content while simultaneously providing substantial growth advantages to the regenerating bladder including increased tissue vascularization and muscle growth in areas of regeneration. This was accompanied by superior bladder functional recovery as demonstrated by urodynamic studies. Finally, treatment AIF-PAs convincingly decreased levels of pro-inflammatory macrophages while positively modulating cytokine expression along with decreasing granuloma- and bladder stone formation. The testing of various permutations of the AIF-PAs will allow the fine tuning of this system in order to better modulate the tissue regenerative response. This will involve the altering of peptide epitope distribution per area on the AIF-PAs as the high density at which these peptides were expressed more than likely contributed to potent tissue regeneration.

Supplementary Material

Refer to Web version on PubMed Central for supplementary material.

Acknowledgments

Peptide amphiphile synthesis was performed in the Peptide Synthesis Core Facility of the Institute for BioNanotechnology in Medicine (IBNAM) at Northwestern University. The U.S. Army Research Office, the U.S. Army Medical Research and Materiel Command, and Northwestern University provided funding to develop this facility. SIS is supported by NIH awards from the National Institute of Biomedical Imaging and Bioengineering (R01EB003806) and the National Institute of Dental and Craniofacial Research (R01DE015920). The content is solely the responsibility of the authors and does not necessarily represent the official views of the NIH.

References

[1]. Montesano R, Orci L. Transforming growth factor beta stimulates collagenmatrix contraction by fibroblasts: implications for wound healing. Proc Natl Acad Sci U S A. 1988; 85:4894–7. [PubMed: 3164478]

[2]. Velnar T, Bailey T, Smrkolj V. The wound healing process: an overview of the cellular and molecular mechanisms. J Int Med Res. 2009; 37:1528–42. [PubMed: 19930861]

[3]. Oberpenning F, Meng J, Yoo JJ, Atala A. De novo reconstitution of a functional mammalian urinary bladder by tissue engineering. Nat Biotechnol. 1999; 17:149–55. [PubMed: 10052350]

[4]. Tili E, Michaille JJ, Wernicke D, Alder H, Costinean S, Volinia S, et al. Mutator activity induced by microRNA-155 (miR-155) links inflammation and cancer. Proc Natl Acad Sci U S A. 2011; 108:4908–13. [PubMed: 21383199]

[5]. Serhan CN, Savill J. Resolution of inflammation: the beginning programs the end. Nat Immunol. 2005; 6:1191–7. [PubMed: 16369558]

[6]. ten Broek RP, Issa Y, van Santbrink EJ, Bouvy ND, Kruitwagen RF, Jeekel J, et al. Burden of adhesions in abdominal and pelvic surgery: systematic review and metanalysis. BMJ. 2013; 347:f5588–603. [PubMed: 24092941]

[7]. Datta A, Scotton CJ, Chambers R. Novel therapeutic approaches for pulmonary fibrosis. Br J Pharmacol. 2011; 163:141–72. [PubMed: 21265830]

[8]. Hartgerink JD, Beniash E, Stupp SI. Self-assembly and mineralization of peptide-amphiphile nanofibers. Science. 2001; 294:1684–8. [PubMed: 11721046]

[9]. Webber MJ, Tongers J, Newcomb CJ, Marquardt KT, Bauersachs J, Losordo DW, et al. Supramolecular nanostructures that mimic VEGF as a strategy for ischemic tissue repair. Proc Natl Acad Sci U S A. 2011; 108:13438–43. [PubMed: 21808036]

[10]. Silva GA, Czeisler C, Niece KL, Beniash E, Harrington DA, Kessler JA, et al. Selective differentiation of neural progenitor cells by high-epitope density nanofibers. Science. 2004; 303:1352–5. [PubMed: 14739465]

[11]. Sohn J, Kim TI, Yoon YH, Kim JY, Kim SY. Novel transglutaminase inhibitors reverse the inflammation of allergic conjunctivitis. J Clin Invest. 2003; 111:121–8. [PubMed: 12511595]

[12]. Ashley RA, Palmer BW, Schultz AD, Woodson BW, Roth CC, Routh JC, et al. Leukocyte inflammatory response in a rat urinary bladder regeneration model using porcine small intestinal submucosa scaffold. Tissue Eng Part A. 2004; 15:3241–6. [PubMed: 19374486]

[13]. Sharma AK, Bury MI, Marks AJ, Fuller NJ, Meisner JW, Tapaskar N, et al. A nonhuman primate model for urinary bladder regeneration using autologous sources of bone marrow-derived mesenchymal stem cells. Stem Cells. 2011; 29:241–50. [PubMed: 21732482]

[14]. Miele L, Cordella-Miele E, Mantile G, Peri A, Mukherjee AB. Uteroglobin and uteroglobin-like proteins: the uteroglobin family of proteins. J Endocrinol Invest. 1994; 17:679–92. [PubMed: 7868811]

[15]. Sharma AK, Bury MI, Fuller NJ, Marks AJ, Kollhoff DM, Rao MV, et al. Cotransplantation with specific populations of spina bifida bone marrow stem/progenitor cells enhances urinary bladder regeneration. Proc Natl Acad Sci U S A. 2013; 110:4003–8. [PubMed: 23431178]

[16]. Ashley RA, Roth CC, Palmer BW, Kibar Y, Routh JC, Fung KM, et al. Regional variations in small intestinal submucosa evoke differences in inflammation with subsequent impact on tissue regeneration in the rat bladder augmentation model. BJU Int. 2010; 105:1462–8. [PubMed: 19863527]

[17]. Sharma AK, Hota PV, Matoka DJ, Fuller NJ, Jandali D, Thaker H, et al. Urinary bladder smooth muscle regeneration utilizing bone marrow derived mesenchymal stem cell seeded elastomeric poly(1,8-octanediol-co-citrate) based thin films. Biomaterials. 2010; 31:6207–17. [PubMed: 20488535]

[18]. Kempf W, Adams V, Wey N, Moos R, Schmid M, Avitabile E, et al. CD68 cells of monocyte/macrophage lineage in the environment of AIDS-associated + and classicsporadic Kaposi sarcoma are singly or doubly infected with human herpesviruses 7 and 6B. Proc Natl Acad Sci U S A. 1997; 94:7600–5. [PubMed: 9207138]

[19]. Khare S, Ratsimandresey RA, de Almeida L, Cuda CM, Rellick SL, Misharin AV, et al. The PYRIN domain-only protein POP3 inhibits ALR inflammasomes and regulates responses to infection with DNA viruses. Nat Immunol. 2014; 15:343–53. [PubMed: 24531343]

[20]. Hazen SL, d'Avignon A, Anderson MM, Hsu FF, Heinecke JW. Human neutrophils employ the myeloperoxidase-hydrogen peroxide-chloride system to oxidize alpha-amino acids to a family of reactive aldehydes. Mechanistic studies identifying labile intermediates along the reaction pathway. J Biol Chem. 1998; 273:4997–5005. [PubMed: 9478947]

[21]. Hernandez-Rodríguez J, Segarra M, Vilardell C, Sanchez M, García-Martínez A, Esteban MJ, et al. Tissue production of pro-inflammatory cytokines (IL-1βeta, TNFαlpha and IL-6) correlates with the intensity of the systemic inflammatory response and with corticosteroid requirements in giant-cell arteritis. Rheumatology. 2004; 43:294–301. [PubMed: 14679293]

[22]. Gessner A, Mohrs K, Mohrs M. Mast cells, basophils, and eosinophils acquire constitutive IL-4 and IL-13 transcripts during lineage differentiation that are sufficient for rapid cytokine production. J Immunol. 2005; 174:1063–72. [PubMed: 15634931]

[23]. Hawkes CA, McLaurin J. Selective targeting of perivascular macrophages for clearance of beta-amyloid in cerebral amyloid angiopathy. Proc Natl Acad Sci U S A. 2009; 106:1261–6. [PubMed: 19164591]

[24]. Souza KL, Gurgul-Convey E, Elsner M, Lenzen S. Interaction between pro-inflammatory and anti-inflammatory cytokines in insulin-producing cells. J Endocrinol. 2008; 197:139–50. [PubMed: 18372240]

[25]. Murray PJ. The primary mechanism of the IL-10-regulated antiinflammatory response is to selectively inhibit transcription. Proc Natl Acad Sci U S A. 2005; 102:8686–91. [PubMed: 15937121]

[26]. Kigerl KA, Gensel JC, Ankeny DP, Alexander JK, Donnelly DJ, Popovich PG, et al. Identification of two distinct macrophage subsets with divergent effects causing either neurotoxicity or regeneration in the injured mouse spinal cord. J Neurosci. 2009; 29:13435–44. [PubMed: 19864556]

[27]. Diegelmann RF, Evans MC. Wound healing: an overview of acute, fibrotic and delayed healing. Front Biosci. 2004; 9:283–9. [PubMed: 14766366]

[28]. Galli SJ, Borregaard N, Wynn TA. Phenotypic and functional plasticity of cells of innate immunity: macrophages, mast cells and neutrophils. Nat Immunol. 2011; 12:1035–44. [PubMed: 22012443]

[29]. Mantovani A, Biswas SK, Galdiero MR, Sica A, Locati M. Macrophage plasticity and polarization in tissue repair and remodelling. J Pathol. 2013; 229:176–85. [PubMed: 23096265]

[30]. Malik AF, Hoque R, Ouyang X, Ghani A, Hong E, Khan K, et al. Inflammasome components Asc and caspase-1 mediate biomaterial-induced inflammation and foreign body response. Proc Natl Acad Sci U S A. 2011; 108:20095–100. [PubMed: 22109549]

[31]. Vacanti NM, Cheng H, Hill PS, Guerreiro JD, Dang TT, Ma M, et al. Localized delivery of dexamethasone from electrospun fibers reduces the foreign body response. Biomacromolecules. 2012; 13:3031–8. [PubMed: 22920794]

[32]. Fujii T, Fuchs BC, Yamada S, Lauwers GY, Kulu Y, Goodwin JM, et al. Mouse model of carbon tetrachloride induced liver fibrosis: histopathological changes and expression of CD133 and epidermal growth factor. BMC Gastroenterol. 2010; 10:79–89. [PubMed: 20618941]

[33]. Gurtner GC, Werner S, Barrandon Y, Longaker MT. Wound repair and regeneration. Nature. 2008; 453:314–21. [PubMed: 18480812]

[34]. Caione P, Capozza N, Zavaglia D, Palombaro G, Boldrini R. In vivo bladder regeneration using small intestinal submucosa: experimental study. Pediatr Surg Int. 2006; 22:593–9. [PubMed: 16773371]

[35]. Slaughenhoupt BL, Mathews RI, Peppas DS, Gearhart JP. A large animal model of bladder exstrophy: observations of bladder smooth muscle and collagen content. J Urol. 1999; 162:2119–22. [PubMed: 10569599]

[36]. Tang L, Eaton JW. Inflammatory responses to biomaterials. Am J Clin Pathol. 1995; 103:466–71. [PubMed: 7726145]

[37]. Ryden L, Molnar D, Esposito M, Johansson A, Suska F, Palmquist A, et al. Early inflammatory response in soft tissues induced by thin calcium phosphates. J Biomed Mater Res A. 2013; 101:2712–7. [PubMed: 23463679]

[38]. Cu A, Ye Q, Sarria R, Nakamura S, Guzman J, Costabel U. N-acetylcysteine inhibits TNF-alpha, sTNFR, and TGF-beta1 release by alveolar macrophages in idiopathic pulmonary fibrosis in vitro. Sarcoidosis Vasc Diffuse Lung Dis. 2009; 26:147–54. [PubMed: 20560295]

[39]. Zhang Y, Lee TC, Guillemin B, Yu MC, Rom WN. Enhanced IL-1 beta and tumor necrosis factor-alpha release and messenger RNA expression in macrophages from idiopathic pulmonary fibrosis or after asbestos exposure. J Immunol. 1993; 150:4188–96. [PubMed: 8473757]

[40]. Bongartz T, Sutton AJ, Sweeting MJ, Buchan I, Matteson EL, Montori V. Anti-TNF antibody therapy in rheumatoid arthritis and the risk of serious infections and malignancies: systematic

review and meta-analysis of rare harmful effects in randomized controlled trials. JAMA. 2006; 295:2275–85. [PubMed: 16705109]

[41]. Chen K, Wei Y, Sharp GC, Braley-Mullen H. Decreasing TNF-alpha results in less fibrosis and earlier resolution of granulomatous experimental autoimmune thyroiditis. J Leukoc Biol. 2007; 81:306–14. [PubMed: 17046971]

[42]. Dinarello CA, van der Meer JW. Treating inflammation by blocking interleukin-1 in humans. Semin Immunol. 2013; 25:469–84. [PubMed: 24275598]

[43]. Gerridzen RG, Thijssen AM, Dehoux E. Risk factors for upper tract deterioration in chronic spinal cord injury patients. J Urol. 1992; 147:416–8. [PubMed: 1732606]

[44]. Zuo L, Tozawa K, Okada A, Yasui T, Taguchi K, Ito Y, et al. A paracrine mechanism involving renal tubular cells, adipocytes and macrophages promotes kidney stone formation in a simulated metabolic syndrome environment. J Urol. 2014; 191:1906–12. [PubMed: 24518782]

[45]. Roupe KM, Nybo M, Sjöbring U, Alberius P, Schmidtchen A, Sørensen OE. Injury is a major inducer of epidermal innate immune responses during wound healing. J Invest Dermatol. 2010; 130:1167–77. [PubMed: 19727116]

[46]. Wynn TA. Common and unique mechanisms regulate fibrosis in various fibroproliferative diseases. J Clin Invest. 2007; 117:524–9. [PubMed: 17332879]

[47]. Grover S, Srivastava A, Lee R, Tewari AK, Te AE. Role of inflammation in bladder function and interstitial cystitis. Ther Adv Urol. 2011; 3:19–33. [PubMed: 21789096]

[48]. Frangogiannis NG, Smith CW, Entman ML. The inflammatory response in myocardial infarction. Cardiovasc Res. 2002; 53:31–47. [PubMed: 11744011]

[49]. Tang TT, Yuan J, Zhu ZF, Zhang WC, Xiao H, Xia N, et al. Regulatory T cells ameliorate cardiac remodeling after myocardial infarction. Basic Res Cardiol. 2012; 107:232–48. [PubMed: 22189560]

[50]. Inoue M, Arikawa T, Chen YH, Moriwaki Y, Price M, Brown M, et al. T cells down-regulate macrophage TNF production by IRAK1-mediated IL-10 expression and control innate hyperinflammation. Proc Natl Acad Sci U S A. 2014; 111:5295–300. [PubMed: 24706909]

[51]. Deng GM, Beltran J, Chen C, Terhorst C, Tsokos GC. T cell CD3z deficiency enables multiorgan tissue inflammation. J Immunol. 2013; 191:3563–7. [PubMed: 23980209]

[52]. Azouz A, Razzaque MS, El-Hallak M, Taguchi T. Immunoinflammatory responses and fibrogenesis. Med Electron Microsc. 2004; 37:141–8. [PubMed: 15449105]

[53]. Park JE, Barbul A. Understanding of the role of immune regulation in wound healing. Am J Surg. 2004; 187:11S–6S. [PubMed: 15147986]

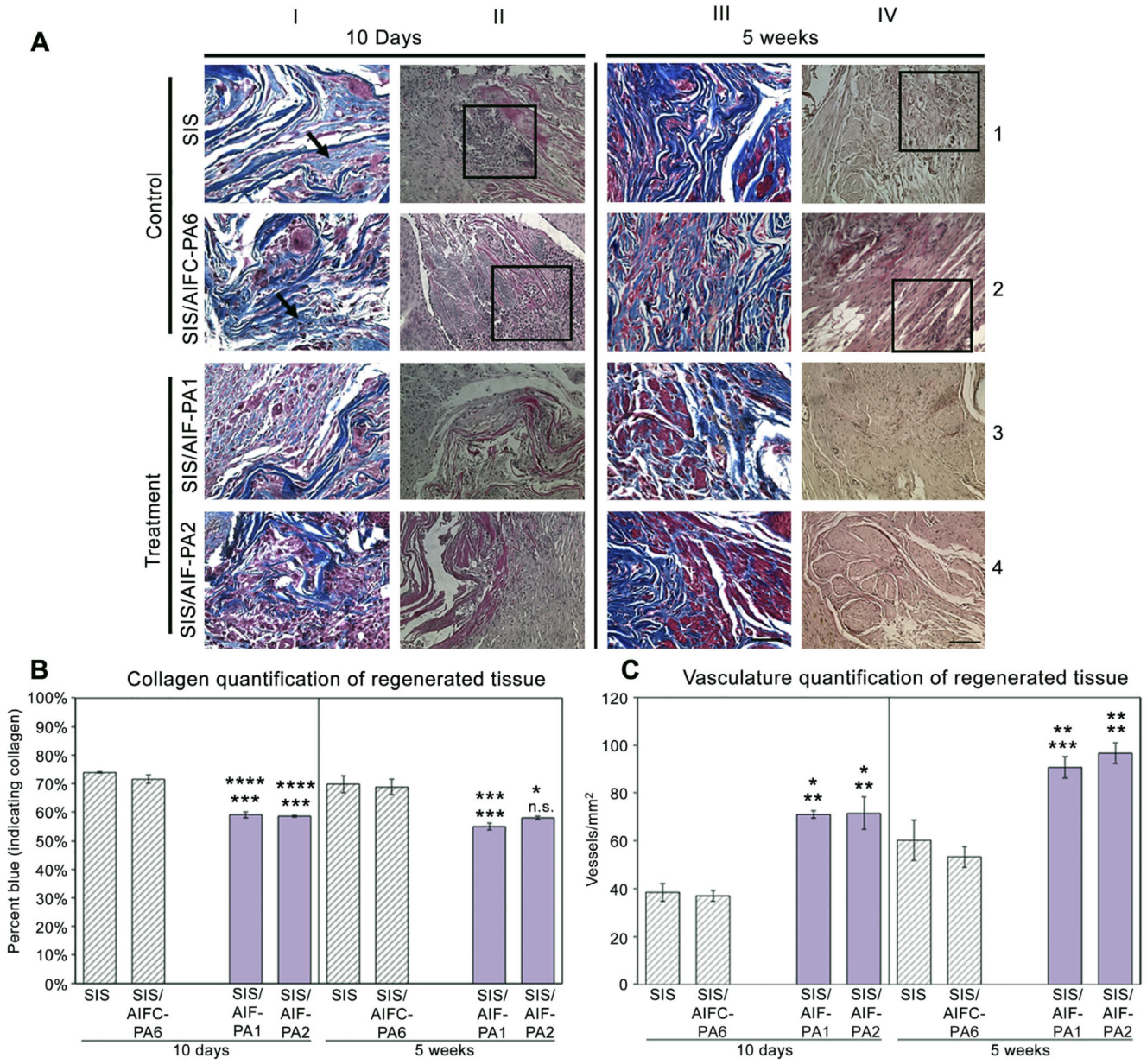

Fig. 1.

Histological and morphometric analyses of augmented bladder tissue. (A) Treatment groups demonstrated near-normal physiological collagen content while control group specimens exhibited higher levels of collagen which remained elevated through 5W. Organized muscle fascicle formation was most notable in treatment groups while still disorganized in control groups at 5W. Magnification is 400× (scale bar, 50 μm) and 200× (scale bar, 100 μm) for Trichrome and H&E stained samples, respectively. (B) Collagen quantification revealed statistically lower levels of collagen deposition in regenerating bladder in treatment vs. control groups over both time-points. (C) An approximate 2× increase in blood vessel numbers of treatment groups vs. control groups at 10D was observed with an approximate 1.5× increase in the treatment groups at 5W. Data shown as means ± SE. Significance

shown for comparison of SIS/AIF-PA1 and SIS/AIF-PA2 to SIS (top) and SIS/AIFC-PA6 (bottom); ****$P \leq 0.0001$, ***$P < 0.001$, **$P < 0.01$, *$P < 0.05$, n.s. non-significant.

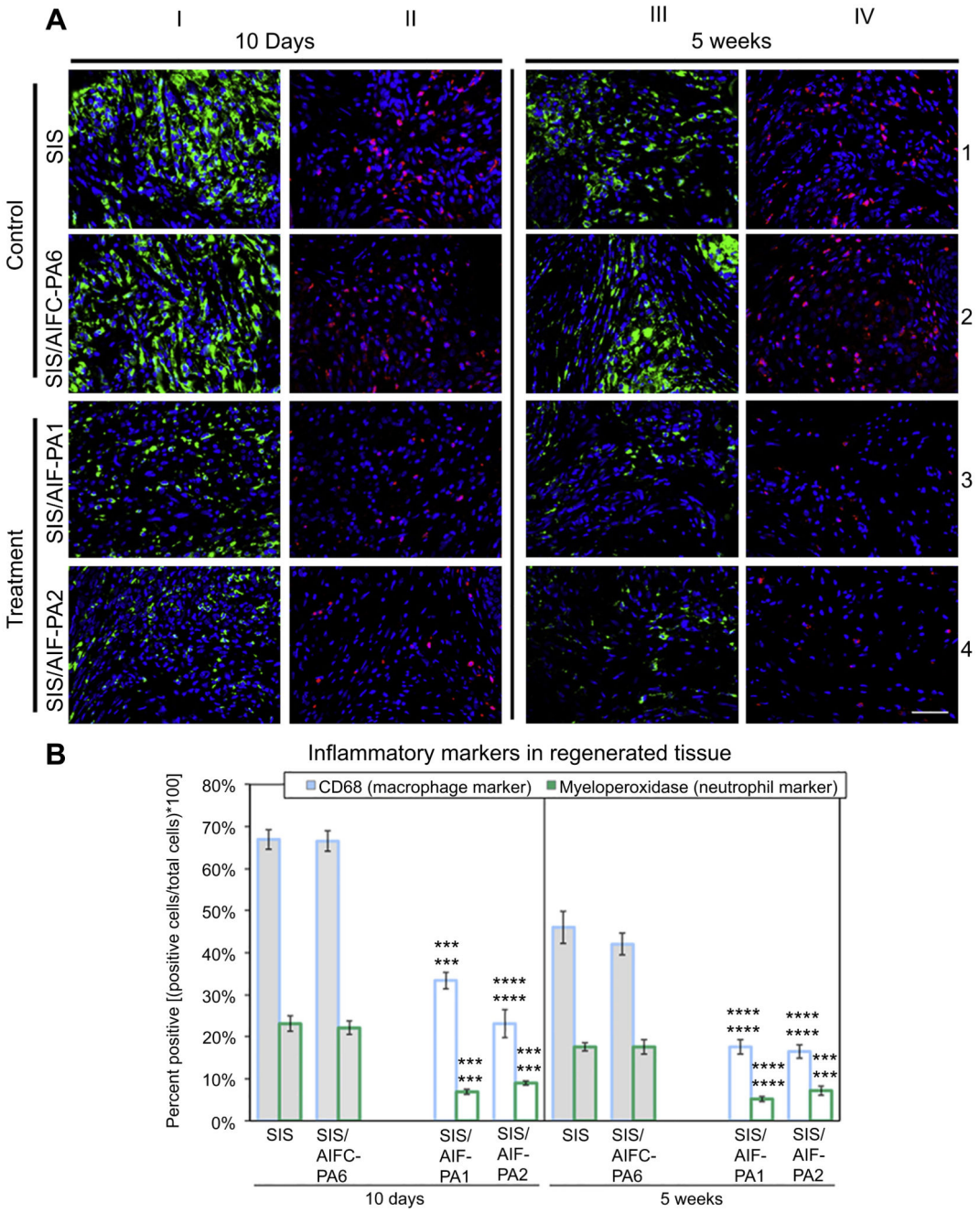

Fig. 2.

Innate immune cell distribution in regenerating bladder tissue. (A) Elevated levels of $CD68^{+}$ macrophages (green) and MPO^{+} neutrophils (red) were evident in the control groups at the 10 day time-point. Although the levels of macrophage and neutrophil infiltrate decreased by 5W, significant levels of both populations still presided in the tissues. Conversely, treatment groups demonstrated a significant decline in macrophage and neutrophil levels at both time-points compared to control groups. Blue, DAPI. Magnification is 400× (scale bar, 50 μm). (B) Quantification of macrophages and neutrophils in augmented tissues demonstrated a

marked decrease in both populations at 10D and 5W in treatment groups. Data shown as means ± SE. Significance shown for comparison of SIS/AIF-PA1 and SIS/AIF-PA2 to SIS (top) and SIS/AIFC-PA6 (bottom); ****$P \leq 0.0001$, ***$P < 0.001$.(For interpretation of the references to colour in this figure legend, the reader is referred to the web version of this article.)

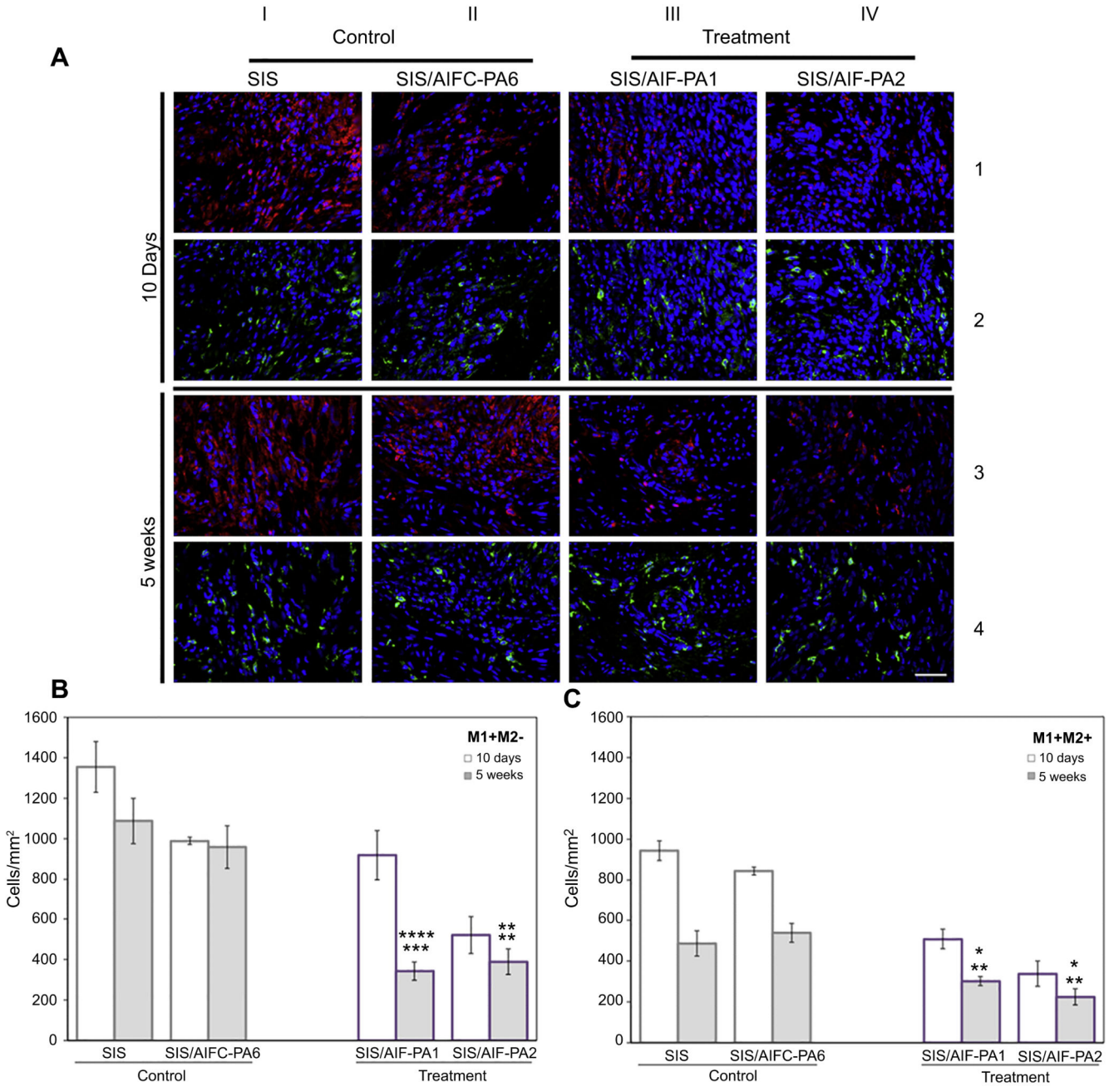

Fig. 3.

M1 and M2 macrophage characterization. (A) Dense populations of $CD86^+$ M1 macrophages (red) were visualized at both time-points post-augmentation throughout the grafted area. This was accompanied by depressed levels of $CD206^+$ M2 macrophages (green) of the control groups, most notably at 5W. Treatment groups saw a significant reduction in $CD86^+$ M1 macrophage presence at 5W coupled with sustained expression of $CD206^+$ M2 macrophages along the entirety of the graft. AIF-PA2 appeared to have a greater impact on macrophage populations than AIF-PA1. Blue, DAPI. Magnification is 400× (scale bar, 50 μm). (B) $M1^+$ macrophages persisted at high levels in control groups

while the SIS/AIF-PA1 treatment group demonstrated a significant decline over time. Data shown as means ± SE. Significance shown for comparison of SIS/AIF-PA1 and SIS/AIF-PA2 to SIS (top) and SIS/AIFC-PA6 (bottom); ****$P < 0.0001$, ***$P < 0.001$, **$P < 0.01$. (C) A general decrease in levels of $M2^+$ macrophages was seen in both control and treatment groups at both time-points but $M2^+$ macrophages were still abundant in treatment groups. Data shown as means ± SE. Significance shown for comparison of SIS/AIF-PA1 and SIS/AIF-PA2 to SIS (top) and SIS/AIFC-PA6 (bottom); ****$P < 0.0001$, **$P < 0.01$, *$P < 0.05$. (For interpretation of the references to colour in this figure legend, the reader is referred to the web version of this article.)

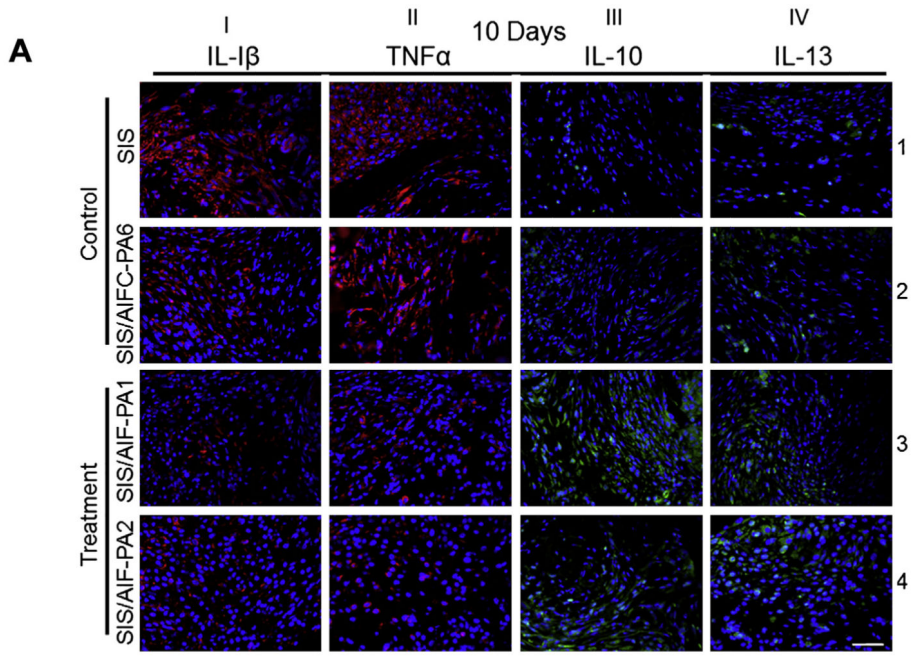

B

Cytokine expression (shown as percentage of cells staining positive)		Pro-inflammatory		Anti-inflammatory	
		IL-1β	TNFα	IL-10	IL-13
Control	SIS	56.7 ± 5.0	63.1 ± 2.6	22.0 ± 2.6	24.8 ± 2.5
	SIS/AIFC-PA6	63.3 ± 2.4	65.1 ± 5.1	27.8 ± 3.0	28.6 ± 3.0
Treatment	SIS/AIF-PA1	28.2 ± 2.4 **/***	32.8 ± 2.5 **/**	52.0 ± 3.1 **/**	48.2 ± 2.8 **/**
	SIS/AIF-PA2	21.2 ± 2.4 ***/***	26.3 ± 2.5 ***/***	56.2 ± 3.4 **/**	41.2 ± 2.2 * / n.s.

Fig. 4.

Pro- and anti-inflammatory cytokine expression. (A) 10D bladder tissue staining with antibodies against the pro-inflammatory cytokines IL-1β (red) and TNFα (red) (columns I and II) demonstrated high levels of expression in control groups but a significant reduction in treatment groups. Conversely, elevated levels of anti-inflammatory cytokines IL-10 (green) and IL-13 (green) were found in treatment groups (columns III and IV, rows 3 and 4) while expression was considerably less in control samples. Blue, DAPI. Magnification is 400× (scale bar, 50 mm). (B) Quantified data revealed an approximate halving of pro-inflammatory cytokine expression when comparing control and treatment groups while anti-inflammatory cytokine expression was higher in treatment groups during this phase of tissue remodeling. ***$P < 0.001$, **$P < 0.01$, *$P < 0.05$. n.s. = non-significant. (For interpretation of the references to colour in this figure legend, the reader is referred to the web version of this article.)

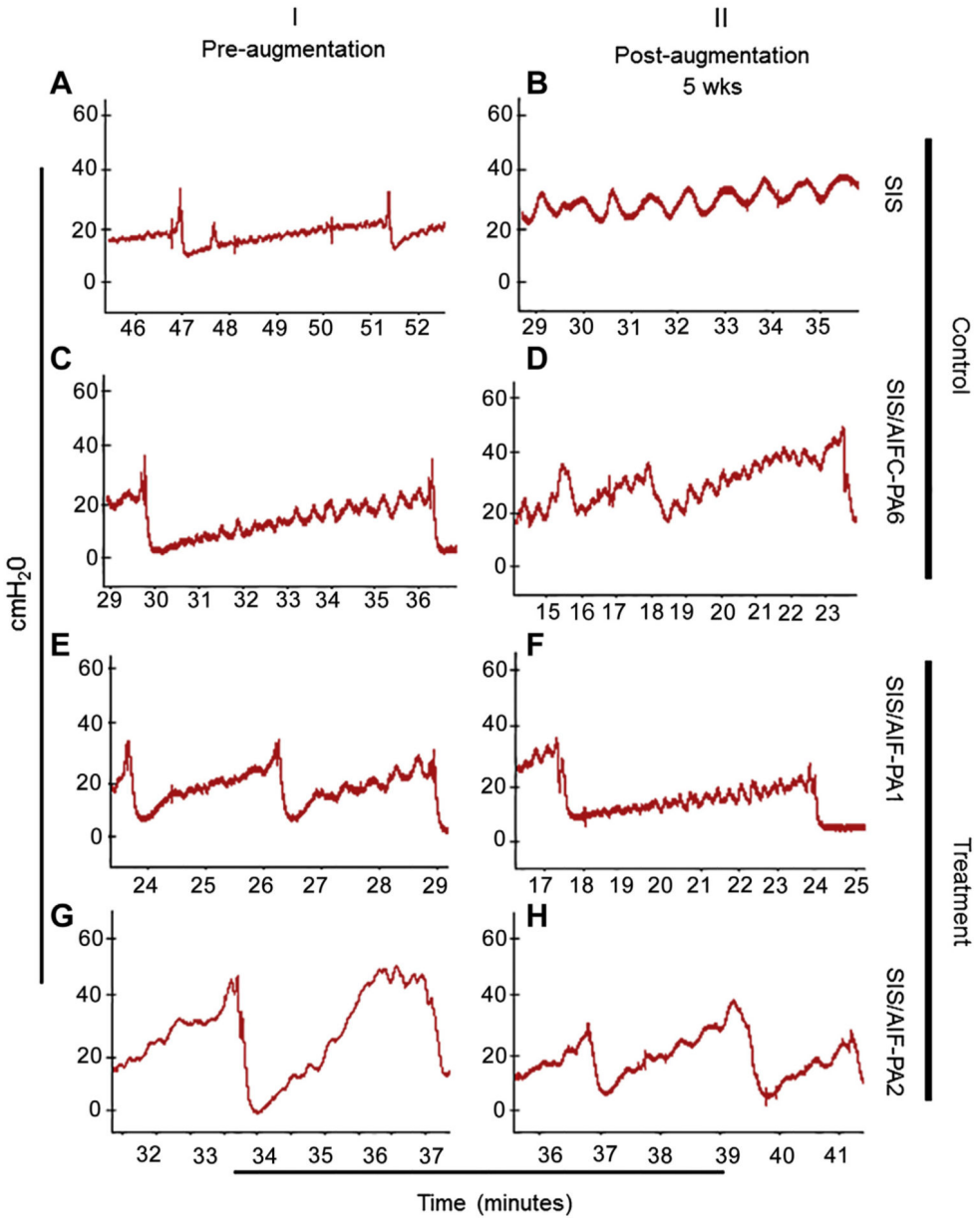

Fig. 5.

Urodynamic studies. UDS testing provided physiological bladder data in the form of bladder pressures and voiding patterns. A similar pattern of bladder filling/voiding was observed amongst animals in the pre-augmentation group (panels A, C, E, G). Decreased bladder compliance was observed in the control groups post-augmentation (panels B, D) while SIS/AIF-PA1 led to higher bladder compliance and decreased intravesical pressures (panel F). SIS/AIF-PA2 treated animals exhibited improved bladder compliance accompanied by a very modest decrease in bladder intravesical pressure (panel H).